International Journal of Statistics: Advances in Theory and Applications
Vol. 1, Issue 1, 2020, Pages 93-110
Published Online on August 03, 2019

http://jyotiacademicpress.org

A COMPARISON STUDY OF STATISTICAL TRACTOGRAPHY METHODOLOGIES FOR DIFFUSION TENSOR IMAGING

LYUDMILA SAKHANENKO and MICHAEL DELAURA

Department of Statistics and Probability
Michigan State University
East Lansing
MI 48824-1027
USA
e-mail: luda@stt.msu.edu

Abstract

We compare two recently developed statistical tractography methodologies by Carmichael and Sakhanenko [2, 3] on a series of artificial but mimicking reality datasets. Both methodologies are used to model diffusion tensor imaging (DTI) and high angular resonance diffusion imaging (HARDI), which are popular brain imaging techniques. The approach based on a higher order tensor model dominates the approach based on a standard matrix model in all scenarios including wide and narrow fibers, single and crossing fibers.

1. Introduction

Diffusion tensor imaging (DTI) is a popular in vivo brain imaging technique, allowing for the tracing of neural fibers called axons, the pathways of communication between different regions of the brain. Thus the investigation of brain connectivity is crucial for disease diagnostics, planning of neuro-surgeries, and understanding how the brain ages.

2020 Mathematics Subject Classification: 62P99, 62G99.
Keywords and phrases: integral curve, tractography.
Research was partially supported by AGEP supplement to the NSF grant DMS-1208238.
Received February 3, 2017

The observed data is related to the axons geometry in a very complicated physical, mathematical and ultimately statistical way. Many tractography methods are available, see [1], [5] and references therein. Recently, a class of so called statistical tractography methods has emerged. It started with the work of Koltchinskii et al. [6], followed by two works of Carmichael and Sakhanenko [2, 3] and, denoted by CS below. These three methodologies rely on 3 different models. The first 2 were compared theoretically and empirically in Carmichael and Sakhanenko [3], who concluded that the later paper provides a statistically better and a more realistic approach. The goal of this paper is to compare empirically the later 2 methods.

First, let us briefly describe the model and the approaches in CS works. Low angular resolution DTI is based on measurements of water diffusion on a grid of points. Locally the relative amount of water diffusion along a spatial direction $b \in \mathbb{R}^3$, $\|b\| = 1$, at a voxel x, $S(x, b)$, is estimated as follows:

$$\log\left(\frac{S(x, b)}{S_0(x)}\right) = - cb^* D^L(x) b + \sigma(x, b)\xi_b,$$

where $S_0(x)$ is the amount of water diffusion without gradient application; $\sigma(x, b) > 0$; ξ_b describes noise; the constant c depends only on the proton gyro-magnetic ratio, the gradient pulse sequence shape, duration and other timing parameters of the imaging procedure; D^L is a 3×3 symmetric positive definite matrix. In practice, a set of N directions b is chosen and the corresponding log-losses are measured. They are stacked into a vector-column Y in model (1). Meanwhile the upper triangular part of matrix D^L is stacked into a 6D vector-column $\mathcal{M}$.

Furthermore, to model the branching phenomenon, Carmichael and Sakhanenko [3] used a mixture of tensors and proposed the following setup: at a fixed location x in a 3D region G we assume that the observations $Y(x) \in \mathbb{R}^N$, $N \geq 6$, arise from a mixture of two underlying

tensors, $\mathcal{M}^{(1)}(x)$ and $\mathcal{M}^{(2)}(x)$. These tensors the same simple maximal eigenvalue but different leading eigenvectors:

$$Y(x) = B(\pi\mathcal{M}^{(1)}(x) + (1 - \pi)\mathcal{M}^{(2)}(x)) + \sum^{1/2}(x)\Xi_x. \tag{1}$$

Here the symmetric tensors $\mathcal{M}^{(i)}(x)$, $i = 1, 2,$ are represented by 6D vectors, B is a fixed known $N \times 6$ design matrix. The random noise 6D vector Ξ has mean 0 and identity covariance matrix. $\sum(x)$ is a positive definite 6×6 unknown matrix. The mixing coefficient π determines the relative contributions of $\mathcal{M}^{(1)}(x)$ and $\mathcal{M}^{(2)}(x)$ to $Y(x)$.

As an alternative approach, Carmichael and Sakhanenko [2] proposed to use a higher order tensor D^H in place of D^L as follows:

$$\log\left(\frac{S(x, b)}{S_0(x)}\right) = -c\sum_{i_1=1}^{3}\cdots\sum_{i_M=1}^{3} D^H_{i_1\ldots i_M}(x)b_{i_1}\ldots b_{i_M} + \sigma(x, b)\xi_b, \tag{2}$$

where $D^H(x)$ with components $D^H_{i_1\ldots i_M}(x)$ is a high-order diffusion tensor, which is a super-symmetrical positive definite $\underbrace{3 \times \ldots \times 3}_{M \text{ times}}$ times tensor with M being an even number. Due to symmetry $D^H(x)$ can be represented by a vector $\mathcal{M}(x) \in R^{J_M}$ with the dimension $J_M = (M + 1)(M + 2)/2$.

Now let $N = J_M m$ for some $m \geq 1$. Then at a fixed location x, one observes log-losses of signal $\log\left(\frac{S(x, b)}{S_0(x)}\right)$ along N directions b, stacked into the vector $Y(x)$, such that

$$Y(x) = B\mathcal{M}(x) + \sum^{1/2}(x)\Xi_x, \tag{3}$$

where $B \in \mathbb{R}^{N \times J_M}$ is a fixed matrix determined from the set of directions b, $Y(x)$, $\Xi_x \in \mathbb{R}^N$ are vectors, the $N \times N$-tensor $\sum(x)$ is symmetric positive definite. This model also tries to accommodate branchings by following all significant pseudo-eigenvectors of D^H simultaneously.

For both models one has a set of locations (typically lying on a regular 3D lattice) $X_1, \cdots, X_n$ at which one observes $Y(X_1), \ldots, Y(X_n)$. The goal is to estimate the integral curves driven by the (pseudo)-eigenvectors $v^{(r)}$, $r = 1, \ldots, R$, of the (super)-tensor field $\mathcal{M}$, which are the solutions of the following ODE:

$$\frac{dx^{(r)}(t)}{dt} = v^{(r)}(x^{(r)}(t)),\ t \geq 0, \quad x^{(r)}(0) = a, \tag{4}$$

or equivalently of the following integral equation: $x^{(r)}(t) = a + \int_0^t v^{(r)}(x^{(r)}(s))ds$. These curves serve as models for the trajectories of fibers within axon fiber tracts.

Carmichael and Sakhanenko [2, 3] proposed natural multi-step estimators for the integral curves that are essentially plug-in estimators. First $\mathcal{M}$ is estimated using the least squares approach, then the (pseudo)-eigenvectors of the estimator are taken as the estimators of the true (pseudo)-eigenvectors, which are then plugged into the main ODE and solved numerically to produce the estimated integral curves. For the first model, a variety of standard clustering techniques can be applied to estimate $\mathcal{M}^{(1)}(x)$ and $\mathcal{M}^{(2)}(x)$ as well as π.

It was shown theoretically that both estimators are asymptotically normal under certain regularity conditions, so they can be traced together with confidence ellipsoids. In this paper, we compare them on artificial but mimicking reality patterns of fiber bundles of various thicknesses under various levels of noise. The first pattern consists of one

fiber bundle which resembles the letter C, so we denote it as such. The second pattern mimics a fiber that branches into two fibers, so the three bundles comprise the letter Y shape. The third pattern mimics the crossing of two fiber bundles which are not orthogonal, so it resembles the letter X. Figure 1 shows these patterns together with reference points on the curves that will be used to assess the quality of the estimation.

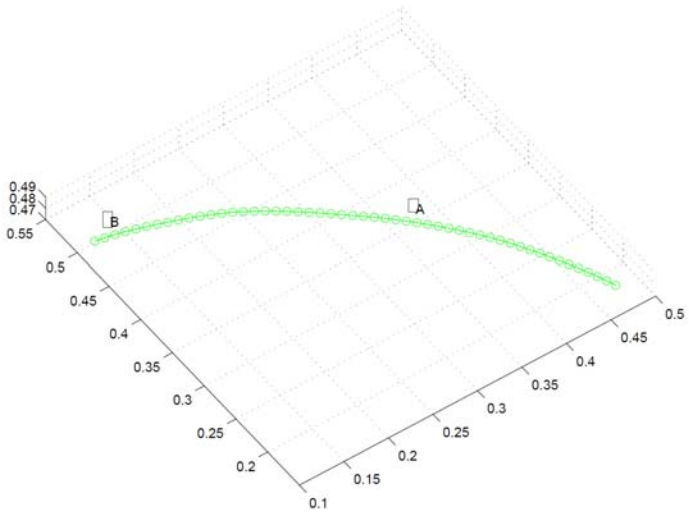

(a) Fibers are estimated using CS procedure for C pattern.

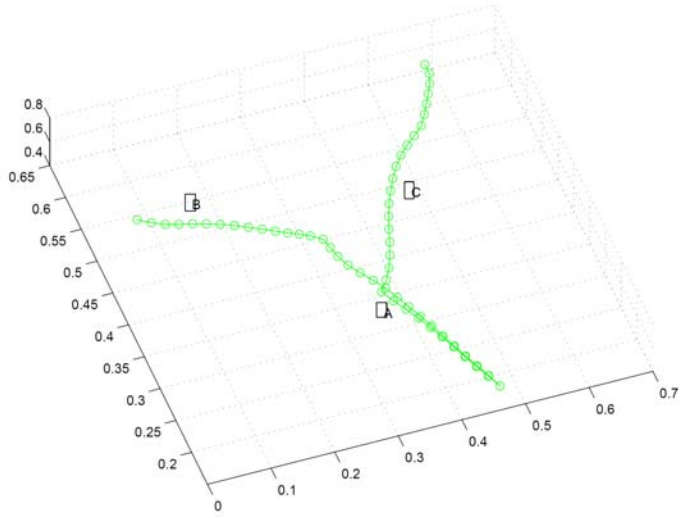

(b) Fibers are estimated using CS procedure for Y pattern.

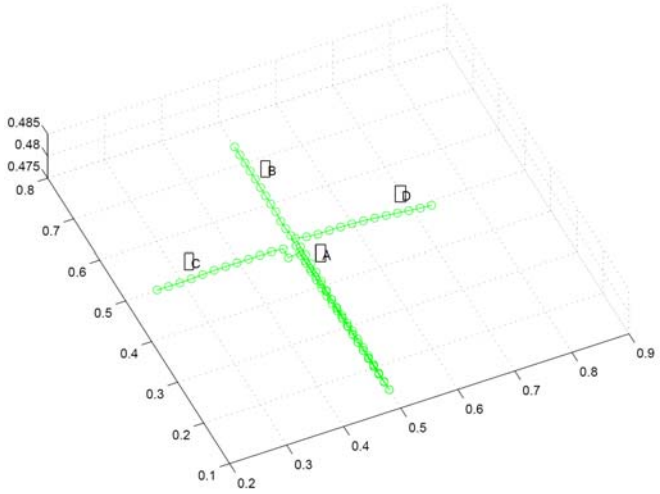

(c) Fibers are estimated using CS procedure for X pattern.

Figure 1. Reference images of typical curves for patterns C, X, and Y.

2. Main Results and Discussion

For each pattern, we consider 4 different bundle thicknesses δ, 2δ, 4δ, and 8δ with $\delta = 0.02$ for images in the volume $[0, 1]^3$. Also, we consider 4 different levels of noise in the models with corresponding signal-to-noise ratios (SNR) 2.5, 5, 7.5, and 10. For both models the tensor fields are generated as follows. First, the (pseudo)-eigenvectors are generated inside the fiber bundles and outside, then the corresponding tensor fields are constructed with eigenvalues [4, 2, 1]. Subsequently, the Gaussian noise of the proper SNR is added in (1) and (3). For the second model, we use the order $M = 4$ with one (for C) and two (for Y and X) significant pseudo-eigenvalues.

Figure 2 shows the estimated curves based on the first model together with their point-wise 95% confidence ellipsoids for the first model. The second model produces similar graphs which are omitted here to save space.

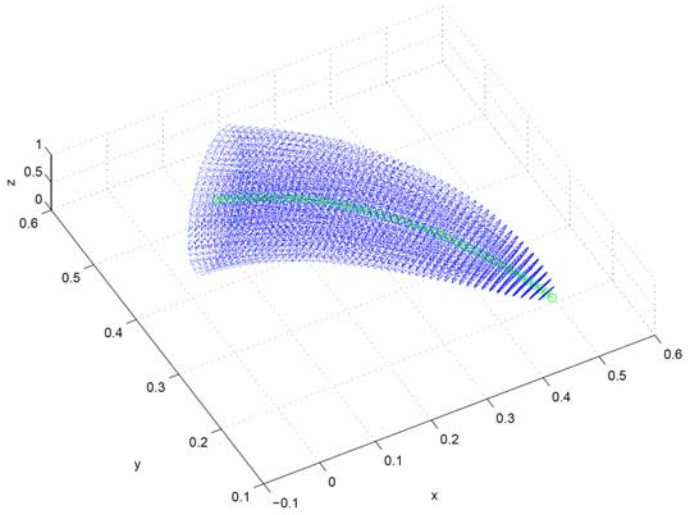

(a) Fibers are estimated using CS procedure for C pattern.

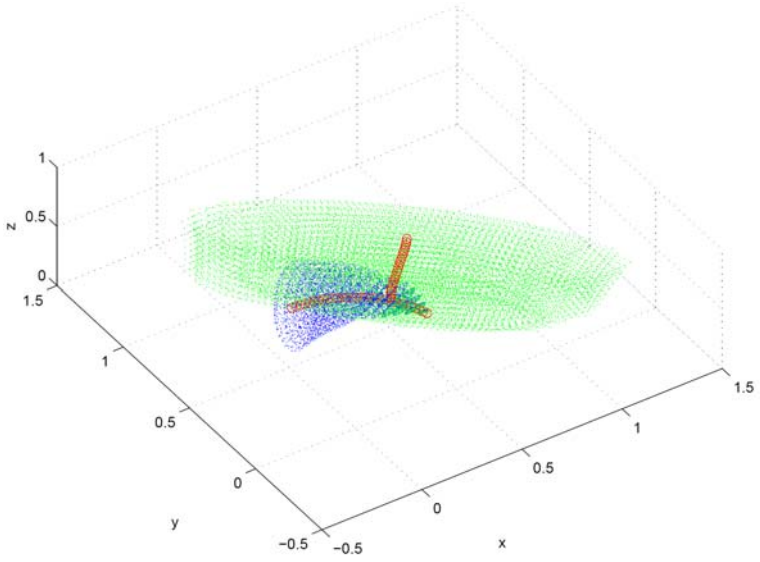

(b) Fibers are estimated using CS procedure for Y pattern.

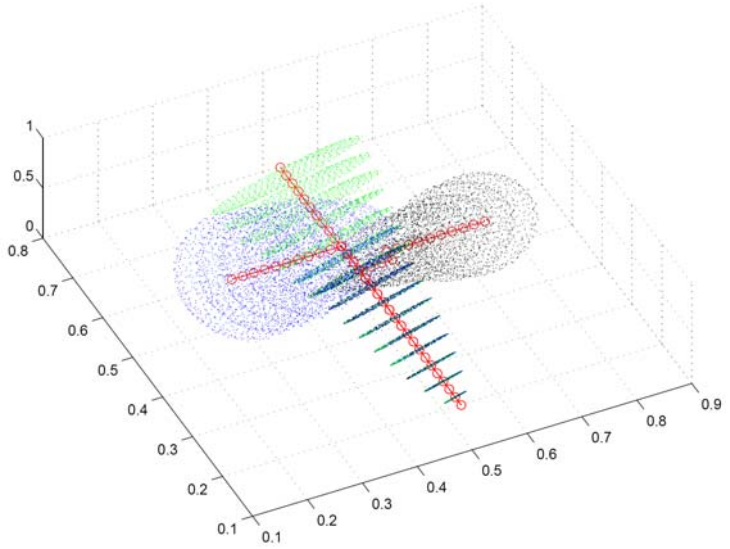

(c) Fibers are estimated using CS procedure for X pattern.

Figure 2. Estimators of typical curves with 95% confidence ellipsoids for patterns C, X, and Y. The first model was used.

Figure 3 demonstrates the so-called p-value maps that could be used in place of heat maps that are popular for images obtained through probabilistic tractography methods. On these images colour represents the p-value for the test of the null hypothesis that a fiber started at the seed point would reach the given point. The cooler colour indicates the rejection of the hypothesis, so the seed point and these points are not connected by a fiber.

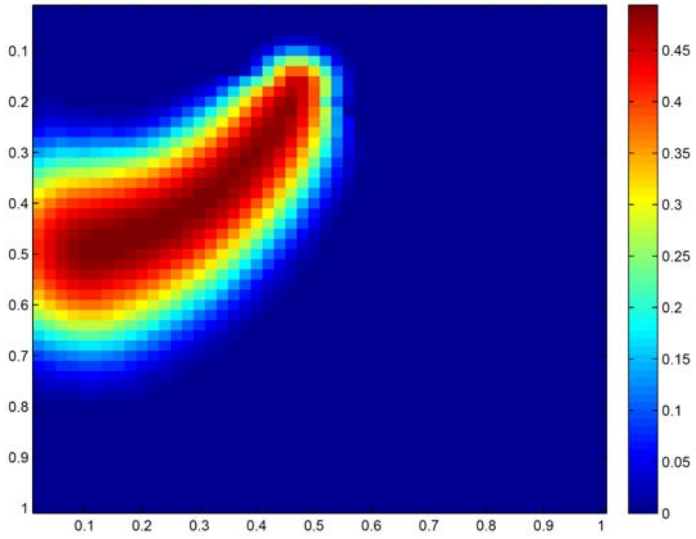

(a) Fibers are estimated using CS procedure for C pattern.

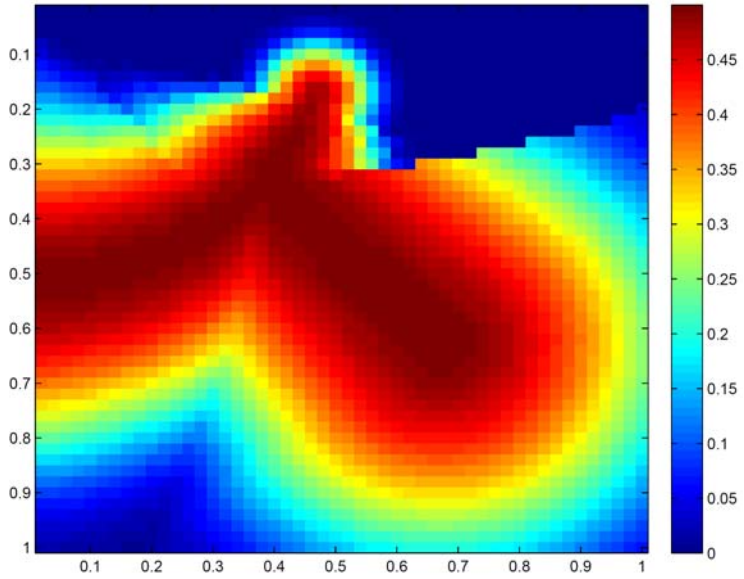

(b) Fibers are estimated using CS procedure for Y pattern.

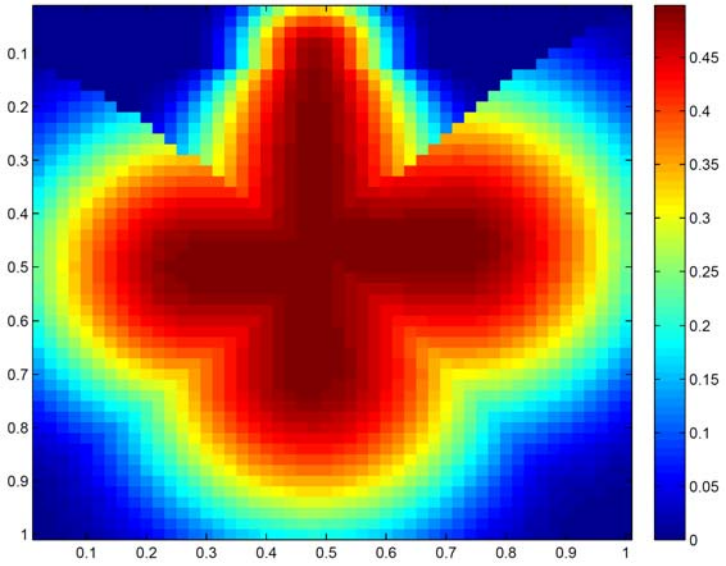

(c) Fibers are estimated using CS procedure for X pattern.

Figure 3. *P*-value maps of typical curves for patterns C, X, and Y. The first model was used.

Overall, the second method produces tighter confidence ellipsoids across all patterns and all levels of thickness as Tables 1 and 2 demonstrate. They give the maximal width of the confidence ellipsoids at the locations labelled on Figure 1. There are two such locations for pattern C: the beginning (A) and the end (B). There are three such locations for pattern Y: the branching point (A) and the ends of the two branches (B) and (C). Similarly, there are four such locations for pattern X: the crossing point (A), the end of the leading fiber (C) and the ends of the secondary fiber (B) and (D). The second method yields tighter confidence ellipsoids by a factor of 10 for many combinations of thickness levels and SNR levels. It is quite noticeable for thickness levels of 2δ and 4δ.

Table 1. The maximal widths of the 95% confidence ellipsoids at the specified points for each of the estimated curves under different thicknesses and with different SNR. Here $\delta = 0.02$, centered Gaussian noise was added to 3 different patterns: C, Y, X; (0.47, 0.1706, 0.48) is the initial point for C and Y; (0.48, 0.2, 0.48) is the initial point for X. The grid is regular with $50 \times 50 \times 50$ knots. $G = [0, 1]^3$. The low angular resolution DTI model is used

Curve type	A	B	A	B	C	A	B	C	D
1δ, SNR = 2.5	.0107	.0145	.2081	.2466	.5485	.1822	.3216	.2009	.2719
1δ, SNR = 5	.0076	.0092	.0569	.1432	.5251	.3128	.3381	.2177	.3263
1δ, SNR = 7.5	.0070	.0084	.0289	.0411	.4489	.1347	.1879	.0769	.2859
1δ, SNR = 10	.0068	.0082	.0197	.0529	.4172	.2202	.2711	.1002	.3538
2δ, SNR = 2.5	.0105	.0144	.0354	.1037	.1100	.0319	.0461	.0638	.0919
2δ, SNR = 5	.0075	.0091	.0111	.0203	.1257	.0100	.0165	.0179	.1023
2δ, SNR = 7.5	.0070	.0084	.0094	.0322	.1145	.0220	.0235	.0199	.0153
2δ, SNR = 10	.0068	.0082	.0085	.0148	.0714	.0041	.0081	.0125	.0080
4δ, SNR = 2.5	.0086	.0106	.0247	.0574	.4765	.0889	.1133	.0560	.2602
4δ, SNR = 5	.0072	.0087	.0134	.0863	.5185	.0218	.0839	.0394	.0591
4δ, SNR = 7.5	.0069	.0082	.0102	.0898	.4702	.0152	.0485	.0203	.0271
4δ, SNR = 10	.0067	.0080	.0084	.0299	.3809	.0042	.0440	.0089	.0108
8δ, SNR = 2.5	.0086	.0106	.0302	.2329	.5677	.0970	.1379	.1342	.1722
8δ, SNR = 5	.0071	.0087	.0116	.0769	.4711	.0866	.2961	.2570	.1483
8δ, SNR = 7.5	.0069	.0082	.0117	.1058	.5196	.0199	.1788	.0193	.1433
8δ, SNR = 10	.0067	.0081	.0097	.0607	.4548	.0140	.1408	.0921	.1473

Table 2. The maximal widths of the 95% confidence ellipsoids at the specified points for each of the estimated curves under different thicknesses and with different SNR. The HARDI model is used

Curve type	A	B	A	B	C	A	B	C	D
1δ, SNR = 2.5	.0032	.0169	.0037	.0683	.1322	.1021	.1021	.3201	.8509
1δ, SNR = 5	.0114	.0197	.0004	.0112	.0018	.0019	.0706	2.00E–7	.0007
1δ, SNR = 7.5	.00002	0.00003	.00005	.0063	.0591	.0100	.0001	.0005	.0496
1δ, SNR = 10	.0053	.0053	.0002	.0021	.0269	.0024	.0040	.0035	.0973
2δ, SNR = 2.5	.0028	.0028	7.61E–6	.0006	.0424	.00002	.0027	.00002	.0238
2δ, SNR = 5	.0001	.0002	2.02E–7	.0002	.0155	9.14E–8	.0092	.0008	.0626
2δ, SNR = 7.5	.0003	.0004	8.93E–8	.00005	.0164	1.34E–8	6.94E–8	1.18E–7	.0087
2δ, SNR = 10	5.87E–6	5.89E–6	1.90E–8	.00002	.0179	2.79E–7	2.79E–7	.00002	.0102
4δ, SNR = 2.5	7.18E–6	8.71E–6	.0031	.0354	.0130	4.75E–6	.00002	6.50E–6	.0092
4δ, SNR = 5	.0001	.0002	.0001	.0001	.0104	.0001	.00001	1.53E–6	.0101
4δ, SNR = 7.5	1.39E–6	.00006	3.88E–8	.00009	.0115	2.62E–8	7.91E–6	.0008	.0079
4δ, SNR = 10	.00001	.0003	.0002	.0003	.0125	.0005	.0006	5.97E–8	.0139
8δ, SNR = 2.5	.0004	.0005	.00001	.0007	.0526	2.25E–6	.0001	.00003	.0246
8δ, SNR = 5	.00002	.00003	2.00E–9	1.29E–7	.0092	7.57E–8	1.64E–7	2.47E–6	.0096
8δ, SNR = 7.5	3.11E–7	3.67E–7	3.17E–9	1.29E–7	.0076	1.28E–8	2.05E–8	2.05E–8	.0001
8δ, SNR = 10	5.18E–6	.0001	1.58E–9	.0005	.0104	3.13E–9	3.15E–9	4.29E–9	.0106

For pattern C, the width increases slightly as one moves along the estimated curve which indicates greater uncertainty. Such behaviour is expected. For pattern Y the width increases greatly after the branching, with the width of ellipsoids for branch C significantly higher than that of branch B. The method is more confident in branch B than in the location of branch C. For pattern X, the crossing point and the end of the leading fiber have confidence ellipsoids of similar widths, increasing slightly towards the end, while the secondary fiber has much wider confidence ellipsoids at both ends. The level of thickness does not affect pattern C, but does influence X and Y (particularly, at smallest width 2δ). Too wide (8δ) or too narrow (δ) fibers are more difficult to estimate. Quite naturally, the confidence ellipsoids are rather wide. These tendencies hold for both methods.

On the contrary, the confidence ellipsoids tend to get tighter as the SNR increases, which is quite expected. For a single fiber, the improvement is especially pronounced when the SNR is increased from 2.5 to 5. For the pattern Y, the improvement is significant when the SNR is increased from 5 to 7.5. For the pattern X, the numbers for the leading fiber A and C follow pattern C's tendencies, while the secondary fibers generally have wider confidence ellipsoids across all levels of thickness, all levels of SNR and both methods. The estimation is not very stable for one of the ends of the secondary fiber especially in the case of high noise, i.e., with SNR of 2.5, and narrow fiber bundle, i.e., with thickness of δ.

Next we consider imaging features of the estimators. It is quite common for probabilistic tractography methods to provide so called occupation probability plots, since these methods are based on Bayesian modelling of the distribution of the fibers. Both approaches being studied in this paper are nonparametric and non-Bayesian. So we need a suitable counterpart to occupation probabilities. We consider the so called p-value map for the image. The null hypothesis at a point x is that a fiber bundle starting at the initial point reaches that point x, in other words the initial point and point x are connected by a fiber. Thus low p-values lead to the

rejection of the connectivity hypothesis. When p-values are calculated at each point x on a grid and a corresponding heat map is made, then we obtain the p-value map. For each pattern, each level of thickness and each level of SNR we calculate the average p-value in an ε-cylinder around the true curve bundle and the average outside of this cylinder. The resulting numbers are summarized in Tables 3 and 4 for the two models. The average p-values are significantly lower outside the ε-tube around the fiber for both models, at all levels of thickness and with all levels of SNR. The ratio of the average p-values inside and outside the ε-tube is at least 10 for the single fiber C for the first model for all levels of thickness and SNR and for the second model for most levels of thickness and SNR. For pattern Y, the ratio is between 1.25 and 2.25 for the first model and it is between 1.32 and 4.21 for the second model. The ratio tends to increase as SNR increase, which means that as the relative amount of noise decreases the boundary between small p-values and large p-values tends to hug the true fiber closer. Likewise, for pattern X, the ratio is between 1.1 and 3 for the first model and it is between 1.1 and 56 for the second model. The level of thickness affects the ratio of average p-values only slightly. The thick-nesses of 2δ and 4δ seem to give higher ratios for both models. Overall, the method based on the second model often gives higher ratio of the average p-values inside and outside the ε-tube around the true fiber bundle, which puts the second method at advantage.

Table 3. We are using the tube of the radius 0.025, 0.1, 0.05 around the true curve for the pattern C, Y, X, respectively. We are calculating the average p-value inside the tube and outside of it for each of patterns. The low angular resolution DTI model is used

Curve type	C: inside	C: outside	Y: inside	Y: outside	X: inside	X: outside
1δ, SNR = 2.5	0.0531	2.5614E–4	0.4944	0.4199	0.4927	0.4453
1δ, SNR = 5	0.0428	8.2638E–5	0.4878	0.3816	0.4833	0.4016
1δ, SNR = 7.5	0.0396	5.6778E–5	0.4761	0.3371	0.4700	0.3872
1δ, SNR = 10	0.0384	5.0436E–5	0.4694	0.3663	0.4578	0.3762
2δ, SNR = 2.5	0.0586	1.7919E–4	0.4727	0.3325	0.4136	0.2895
2δ, SNR = 5	0.0417	1.0026E–4	0.4461	0.2931	0.3969	0.3115
2δ, SNR = 7.5	0.0395	6.2330E–5	0.4325	0.2855	0.3127	0.1527
2δ, SNR = 10	0.0383	5.2524E–5	0.4157	0.1819	0.2580	0.0813
4δ, SNR = 2.5	0.0560	2.1590E–4	0.4682	0.3431	0.4073	0.2990
4δ, SNR = 5	0.0429	7.3598E–5	0.4404	0.3009	0.3857	0.3417
4δ, SNR = 7.5	0.0397	5.5894E–5	0.4379	0.3448	0.3095	0.1825
4δ, SNR = 10	0.0384	4.8152E–5	0.4357	0.3442	0.3348	0.2700
8δ, SNR = 2.5	0.0554	1.9306E–4	0.4585	0.2844	0.4422	0.4011
8δ, SNR = 5	0.0426	7.6901E–5	0.4413	0.3101	0.4247	0.3980
8δ, SNR = 7.5	0.0394	6.0148E–5	0.4341	0.3144	0.4031	0.3731
8δ, SNR = 10	0.0383	5.0609E–5	0.4340	0.3344	0.3906	0.3776

Table 4. We are using the tube of the radius 0.025, 0.1, 0.05 around the true curve for the pattern C, Y, X, respectively. We are calculating the average *p*-value inside the tube and outside of it for each of patterns. The HARDI model is used.

Curve type	C: inside	C: outside	Y: inside	Y: outside	X: inside	X: outside
1δ, SNR = 2.5	0.0044	4.4549E–4	0.4082	0.3062	0.4858	0.4678
1δ, SNR = 5	0.0042	1.6423E–5	0.2331	0.1473	0.2744	0.1914
1δ, SNR = 7.5	3.5732E–7	3.4434E–7	0.2908	0.1277	0.1952	0.1582
1δ, SNR = 10	0.0176	4.4830E–5	0.2380	0.1557	0.1921	0.1627
2δ, SNR = 2.5	0.0239	2.0300E–7	0.2904	0.2255	0.2006	0.1459
2δ, SNR = 5	1.0994E–5	5.9370E–9	0.2373	0.0651	0.1554	0.1375
2δ, SNR = 7.5	1.277E-5	6.4221E–6	0.0808	0.0389	0.0229	0.0110
2δ, SNR = 10	3.3089E–4	4.1171E–6	0.1267	0.0801	0.0477	0.0382
4δ, SNR = 2.5	2.4452E–5	3.9917E–6	0.3527	0.1639	0.0235	0.0149
4δ, SNR = 5	0.0026	4.8587E–5	0.1428	0.0441	0.0613	0.0558
4δ, SNR = 7.5	2.8126E–4	1.7066E–4	0.1050	0.0299	0.0453	0.0393
4δ, SNR = 10	9.4983E–7	5.7935E–7	0.2358	0.0623	0.0466	0.0359
8δ, SNR = 2.5	0.0022	9.7721E–7	0.2133	0.0772	0.0655	0.0099
8δ, SNR = 5	1.0082E–4	5.1414E–5	0.2042	0.0455	0.0559	0.0501
8δ, SNR = 7.5	2.1534E–4	1.6087E–5	0.1193	0.0283	0.0056	0.0001
8δ, SNR = 10	2.3108E–4	5.6589E–6	0.1959	0.0501	0.1335	0.0422

3. Conclusion

Our empirical comparison of the standard matrix model to the higher order tensor model demonstrates clearly that the higher order tensor model is highly preferable to the former. Regardless of fiber thickness, ratio of signal-to-noise, or tracing pattern, the second method yields tighter confidence ellipsoids, for many combinations of the three by as much as a factor of 10. The first model slightly beats the second for pattern C in the calculation of the ratio of average *p*-values inside and outside the ε-tube. Since the difference is small, combined with the fact that the second model dominates for the more complex patterns Y and X,

the second method is preferred. We last note that both methods have some difficulty in estimating fibers at the extremes of fiber thickness (narrowest fiber thickness or widest fiber thickness), as well as at some locations after branching (in Y and X patterns). With this in mind, we consider estimation of axonal surfaces rather than curves as a possible further area of research.

References

[1] H.-E. Assemlal, D. Tschumperle, L. Brun and K. Siddiqi, Recent advances in diffusion MRI modeling: Angular and radial reconstruction, Medical Image Analysis 15 (2011), 369-396.

[2] O. Carmichael and L. Sakhanenko, Integral curves from noisy diffusion MRI data with closed-form uncertainty estimates, Statistical Inference for Stochastic Processes 19(3) (2016), 289-319.

DOI: https://doi.org/10.1007/s11203-015-9126-9

[3] O. Carmichael and L. Sakhanenko, Estimation of integral curves from high angular resolution diffusion imaging (HARDI) data, Linear Algebra and its Applications 473 (2015), 377-403. Special issue on Statistics.

[4] M.-A. Côté, G. Girard, A. Boré, E. Garyfallidis, J.-C. Houde and M. Descoteaux, Tractometer: Towards validation of tractography pipelines, Med. Image Analysis 17 (2013), 844-857.

[5] A. Daducci, E. Canales-Rodríguez, M. Descoteaux, E. Garyfallidis, Y. Gur, Y.-C. Lin, M. Mani, S. Merlet, M. Paquette, A. Ramirez-Manzanares, M. Reisert, P. Rodrigues, F. Sepehrband, E. Caruyer, J. Choupan, R. Deriche, M. Jacob, G. Menegaz, V. Prčkovska, M. Rivera, Y. Wiaux and J.-P. Thiran, Quantitative comparison of reconstruction methods for intra-voxel fiber recovery from diffusion MRI, IEEE Proc. (2013).

[6] V. Koltchinskii, L. Sakhanenko and S. Cai, Integral curves of noisy vector fields and statistical problems in diffusion tensor imaging: Nonparametric kernel estimation and hypotheses testing, Annals of Statistics 35(4) (2007), 1576-1607.

[7] L. Sakhanenko, Using the tractometer to assess performance of a new statistical tractography technique, Journal of Nature and Science 1(7) (2015), 1-12; e130.

http://www.jnsci.org/content/130

[8] H. Zhu, H. Zhang, J. Ibrahim and B. Peterson, Statistical analysis of diffusion tensors in diffusion-weighted magnetic resonance image data, J. Amer. Statist. Assoc. 102 (2007), 1081-1110.

■